Enhancing performance metrics of an electrical-powered subsea robotic dredging crawler across varied inclination angles

by M.O. Ojumu[1], A.K. Raji[2], E.F. Orumwense[1]

Affiliation:
[1]Mechanical and Mechatronic Engineering Faculty of Engineering and the Built Environment, Cape Peninsula University of Technology, South Africa
[2]Electrical, Electronic, and Computer Engineering Department, Cape Peninsula University of Technology, South Africa

Correspondence to:
M.O. Ojumu

Email:
mikeoluwaseunojumu@gmail.com

Dates:
Received: 23 Apr. 2024
Revised: 13 Jun. 2025
Accepted: 13 Jun. 2025
Published: September 2025

How to cite:
Ojumu, M.O., Kamoru, R.A., Orumwense, E.F. 2025. Enhancing performance metrics of an electrical-powered subsea robotic dredging crawler across varied inclination angles. *Journal of the Southern African Institute of Mining and Metallurgy*, vol. 125, no. 9, pp. 543–554

DOI ID:
https://doi.org/10.17159/2411-9717/3380/2025

Abstract

This research paper introduces a novel passive method for ocean mining using an electric-powered robotic subsea dredging crawler designed to operate in various subsea conditions, including unstructured and rough terrain. The electric-powered robotic subsea dredging crawler is equipped with two driving tracks and features a complex assembly of tank tread chain link, tank tread idler wheels, tank tread sprockets, bronze bushings, motor hub, motor mount, and a 12-volt direct current motor. To evaluate the performance of the electric-powered robotic subsea dredging crawler, it was compared with existing ocean hydraulic exploration crawlers, such as MK3 ROST, in terms of drive performance on an inclined ramp with five angles of inclination (0°, 15°, 20°, 25°, 30°). The experiment aimed to determine the maximum velocity, torque, and efficiency of the crawler at different angles of inclination. The collected data were analysed and plotted using Python, and the effect of the electric-powered robotic subsea dredging crawler's weight on its driving performance was also considered. The results of this study demonstrate a quadratic relationship between driving performance and inclination angle, which can be used to optimise the electric-powered robotic subsea dredging crawler's performance for future ocean mining robot drive applications.

Keywords

subsea crawler, angle of inclination, driving units, and dredging

Introduction

The subsea ocean dredging crawler is a crucial exploration and recovery machine utilised in the mining industry for the excavation and recovery of minerals and associated waste rocks, commonly referred to as undersea gravels, found on the ocean floor. This machine is capable of sinking to the bottom of a body of water and moving about using traction against the seabed with the aid of wheels or tracks. Tethered to a surface ship by cables providing power, control, video, and lifting capabilities, the subsea crawler is an effective tool for deep-sea exploration and mining. The process of ocean excavation involves several fundamental techniques, including ocean floor mapping, mineral location, sampling, sinking of the crawler/piloting, and dredging of the resources. However, traditional hydraulic crawlers like the MK3 ROST have been known to cause ocean pollution and consume high amounts of energy, prompting the development of a scaled-down prototype of an electric-powered robotic subsea dredging crawler (EPRSDC) that is comparable to the MK3 ROST. In this research, we aim to focus on the driving performance of the crawler and how it reacts to different elevational terrains. To achieve this, we will design the EPRSDC and ramp using SOLIDWORKS and assemble the hardware component using the Tetrix max robotics kit. The ramp was manufactured and assembled, and the findings contribute to the advancement of ocean excavation technology.

Materials and structural components using Tetrix max robotics kits

The image in Figure 1 showcases the integration of components from the Tetrix Max robotics kits in the construction of the educational prototype robot for scientific and developmental challenges (EPRSDC). This innovative assembly utilises a variety of components primarily crafted from 1050 aircraft-grade aluminum structural pieces, ensuring durability and reliability in the robot's construction.

The structural components feature meticulously machined channels with trademark patterns, incorporating 3 mm and 8 mm holes. This design allows for versatile connectivity, with holes strategically positioned at multiples of 90° and 450°, offering a high angular attachment, and flexibility during the assembly process. The ability to connect components at these specific intervals enhances the

Figure 1—Tetrix max robotics kit

adaptability of the robot, accommodating diverse configurations to meet the unique requirements of different applications both for land and ocean robotic design prototyping.

The Tetrix Max robotics kits, responsible for the creation of these advanced components, were developed by Pitsco Education. These kits serve a multifaceted purpose, aiming to facilitate both mechanical and electrical design aspects of robotics. Beyond educational applications, they are instrumental in providing training for a wide range of robot types. Moreover, the Tetrix Max kits find application in the creation of research test benching and development purposes, demonstrating their versatility, and contribution to advancing robotic technologies into industrial based solution.

In conclusion, the Figure 1 image offers a glimpse into the sophisticated construction of the EPRSDC, highlighting the utilisation of Tetrix Max robotics kits and their meticulously designed aluminum components. This not only underscores the importance of materials like aircraft-grade aluminum but also emphasises the broader educational and developmental goals achieved through the integration of these cutting-edge robotic components.

Literature review

In the work in Van Bloois et al. (2009) the historical development of dredging and mining technology was critically discussed in the aforementioned. It was noted that the increase in dredging activities in recent years has led to significant improvements in the technology used for seafloor extraction. Compared to several decades ago when technology was limited, conventional dredging equipment can now excavate up to a depth of 300 m towards the ocean floor. The hydraulically powered ocean dredging crawlers currently in use have unique fundamental features, parts, and functions that enable effective deep-sea mining. In a seminal work by Naidoo (2013), he underscored the pivotal role that the mining of natural resources has played in the economic development of South Africa. The evolution of South Africa's mining industry is steeped in a history of apartheid, a system that perpetuated the exploitation of migrant labour and shaped the country's mineral resources within the confines of political, social, and economic paradigms for over 140 years. The authors of this paper provide a critical analysis of the historical changes that have occurred in the country's mining industry, with particular emphasis on the impact of apartheid on the exploitation and extraction of mineral resources. This work serves as an important reference for understanding the complex relationship between the mining industry and the economic development of South Africa.

In the field of hydraulic systems, the occurrence of leaks is a well-known problem that can cause significant hydraulic pollution (Tondolo, 2012). Such leaks can originate both internally and externally to the system and can result in a decrease in its overall drive efficiency. Particularly, external leaks can be hard to detect due to the absence of visual indicators underwater until the system's performance has been compromised substantially. It is worth noting that hydraulic ocean crawlers are prone to internal leakages as a result of wear and tear during operation, which contributes to ocean pollution and cavitation. The formation of cavities in hydraulic ocean mining crawlers is mainly attributed to the collapse of hydraulic oil bubbles resulting from soluble gas solutions, fluid dips, and rapid pressure increase.

According to Haga et al. (2001), the hydraulic ROST excavator comprises three main components, which include the undercarriage, upper structure, and front attachment. The upper structure is responsible for rotating the undercarriage, while the backhoe front attachment consists of three major components, namely the boom, arm, and bucket. The boom is the part of the front attachment that provides the lifting force, while the arm is responsible for the movement of the bucket. The bucket is designed to scoop up the material to be excavated and transfer it to the hopper for transportation. These components work together to enable the hydraulic ROST excavator to efficiently excavate mineral resources from the ocean floor. Nazaruddin and Gunawan (2015) provided an in-depth discussion on the importance of the undercarriage drive system in heavy-duty equipment, particularly in ocean dredging crawlers. The undercarriage is composed of several components that are responsible for the autonomous movement of the excavator, including the sprocket, final drive unit, track shoe, carrier roller, track frame, track chains, and front idler. Of these, the final drive unit plays a crucial role in transmitting power from the geared motor and increasing the torque for the entire track automation. further highlighted that the transmission for the arrangement is powered with a low speed of 3.6 km/h and a maximum speed of 5.5 km/h as a result of a generated motor-driven rotation of 2000 rpm. These findings demonstrate the significant role played by the undercarriage in ensuring effective movement and maneuverability of hydraulic ocean dredging crawlers.

According to Daanen (2017), the development of a model that characterises the interaction between track drive systems and seabed soil was examined. The study utilised an analytical tool to assess the impact of aerometer sensors. Tracked vehicles, also known as tracked equipment, were propelled by electric motors producing rotational motion for forward thrust. The analysis distinguished between two types of track drives, namely flexible and rigid track belts. Flexible tracks were comprised of rubber belts or specific types of steel linked tracks, whereas rigid track belts utilised steel linked tracks. The operational behaviour of both types of track drives was reported to be dissimilar, with the key identifier being the ratio between road wheel spacing and track link length. Track driven vehicles can either have or lack suspension, with the suspension being a single unit for the entire track frame or a distinct unit for each road wheel. The presence of suspension was found to have an impact on the interaction between the track and the soil, which depended on various parameters. Mooney and Johnson (2014) discussed a method for solving the problem of loop closure efficiency in harsh environments using RFID technology for slippage-sensitivities in odometry 2D pose dynamic drive tracking. The proposed approach allows a robot to continuously climb rough terrain, even in unfavourable weather conditions. The

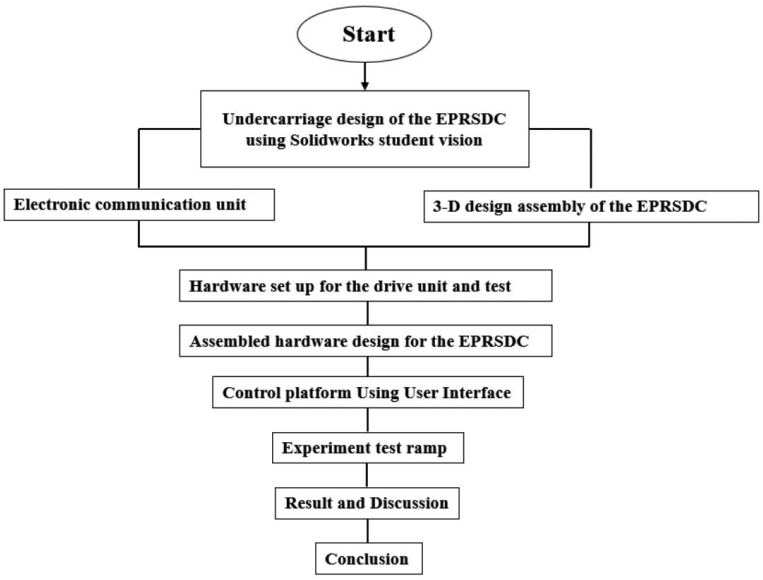

Figure 2—Flowchart of the design paper methodology

angle of elevation was evaluated on a ground driving motor such as the Lurker robot, which is capable of navigating autonomously on rough terrain with ramps and rolls. In the context of ocean exploration, robotic crawler machines are used in areas where the evaluated elevation for their driving unit is coded to its highest estimate. However, in unpredictable environments, these methods may lead to less efficient torque for climbing an open ramp elevation.

Methodology

In this work, a flowchart is used to present the overall study and the methodology employed to achieve the research objectives, as illustrated in Figure 2. The study involved several steps, including 3D design structural modelling of the crawler, hardware assembly, drive test, control system, angular test inclination, data collection, and results analysis.

The first step Involves the 3D design of the EPRSDC hardware, which was assembled into three fundamental parts before the final hardware preliminary design assembly was made using Tetrix max robotics kits. The undercarriage system was subdivided into three components, namely the venturi dredging arm, the driving base, and the internal frame. The total length diameter of the design was 450 mm x 412 mm. The second step involved the hardware assembly, which entailed the fabrication of the components and their assembly into the final design. The third step involved drive test and optimisation, which involved testing the system under different conditions to optimise its performance. The fourth step involved the development of the control system, which enabled the crawler to operate autonomously. The fifth step involved the angular test inclination, which involved testing the crawler's ability to climb and manoeuvre through challenging terrains. The sixth step involved data collection, which was carried out during the drive test and angular test inclination. Finally, the results obtained from the analysed data were used to evaluate the performance of the EPRSDC crawler.

The EPRSDC's framework undercarriage design

The undercarriage system's primary dimension was determined by utilising a range of standardised channel sizes including 32 mm, 96 mm, 160 mm, and 288 mm, as well as various angle, flat, and connector brackets such as 144 mm, 288 mm, L bracket, inside corner bracket, inside C connector, and adjustable angle corner bracket. Additionally, 64 x 16 mm, 69 x 16 mm, 160 x 16 mm, and 288 x 16 mm flats were incorporated into the layout design to produce the final undercarriage configuration.

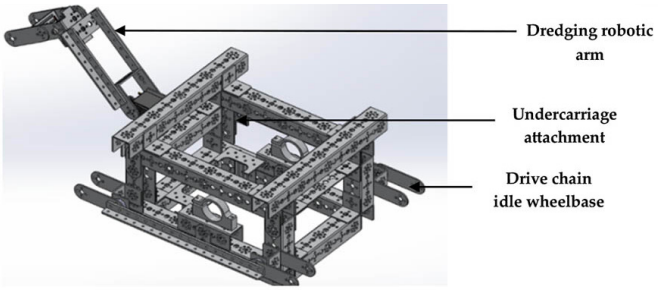

Figure 3—Framework for undercarriage design

Figure 3 depicts the primary structural composition of the design consisting of three sections: The undercarriage, the drive system, and the arm. The frame is constructed using an assortment of materials, including channels, bars, angles, plates, brackets, flats, axles, hubs, spacers, posts, stand-offs, nuts, screws, and fasteners. The 1050 series aircraft grade aluminum was selected as the material for the fabrication of these parts.

Two degrees of freedom boom arm with a venturi dredging nozzle

The ocean dredging machine incorporates a boom arm with specific degrees of freedom. The arm is equipped with an end effector manipulator that enables the dredging and pressure pump nozzles to operate within fixed parameters. To enhance the performance of the machine, a venturi nozzle was developed using 1050 aircraft grade aluminum and was subsequently connected to the 12-volt dredging pump.

Figure 4 depicts a two-degree-of-freedom (2-DOF) boom arm featuring a venturi dredging nozzle. The 2-DOF is regulated by a 6.7-volt DC servo motor that receives control signals from an NI myRIO to the servo control. The purpose of the boom arm's design

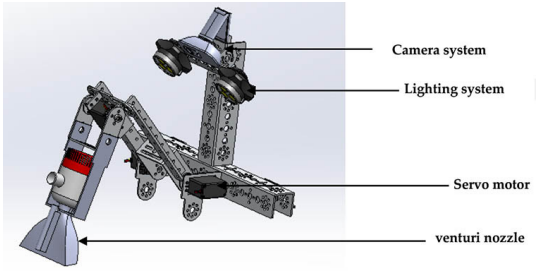

Figure 4—Two-degree-of-freedom boom arm with a venturi dredging nozzle

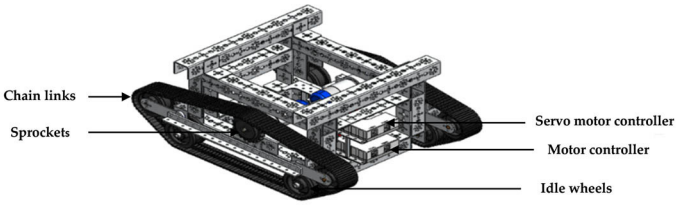

Figure 5—Undercarriage tank tread idler drive system

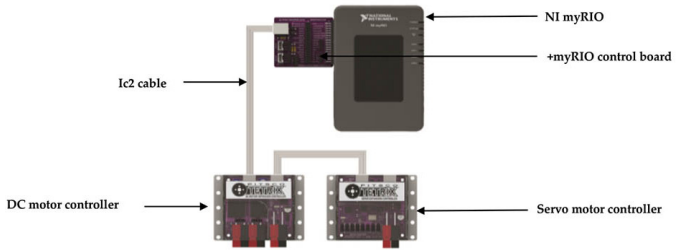

Figure 6—Electric powered robotic subsea crawler

is to facilitate the extraction of materials. Both the boom arm and venturi dredging nozzle were constructed from 1050 series aircraft-grade aluminum. The servo motors were affixed using a servo motor single standard-scale bracket and standard-scale pivot arm with bearings. A 180-degree Dsservo Ds3225 25kg metal gear high torque waterproof digital servo was employed to control the boom arm.

EPRSDC with undercarriage tank tread chain idler drive base

Figure 5 illustrates the structural composition of the electric-powered robotic subsea crawler undercarriage drive system. A 288 mm x 160 mm x 96 mm stand-up pulls boxed frame was specifically designed with a total tank tread chain link of 406 mm in length. The tank tread sprocket was attached to a motor hub, which, in turn was connected to a 12-volt torquenado motor shaft, enabling the track to rotate both clockwise and counterclockwise. Tank tread idle wheels were employed to facilitate parallel drive for the chain link and to design the shape of the crawler drive system. The electronic motor controller was utilised to regulate the 12-volt torquenado motor.

Electronic communication unit

The power system was sourced from a 12-volt 3000 mAh rechargeable NiMH battery pack comprising ten cells. The power supply is directed through an emergency switch to the servo motor controllers, with a wire being looped to the DC motor controllers. Subsequently, a wire was connected from the motor controller to the NI myRIO. Communication between the NI myRIO, motor controller, and servo motor controllers was established via the iC2 cable.

3D assembly design of the EPRSDC

Figure 7 displays the utilisation of SolidWorks for modelling the EPRSDC. This software facilitates the adjustment of individual parts, including the drive units, internal frame, and dredging arm, thereby streamlining the final design assembly process. The scalability of this design renders it suitable for large-scale industrial manufacturing of the EPRSDC. In the case of the scaled-down prototype, all electronic components were precisely positioned using Solidworks mates to achieve a realistic 3D visualisation of the model. The software was instrumental in assembling the three undercarriage systems of the EPRSDC. 3D software is essential for designing the robot's structural and hardware components as it affords complete freedom and flexibility in the development process, from conceptualisation of the design to hardware manufacturing.

Setup for the drive unit

As depicted in Figure 8, the test bench connection of the driving system for the EPRSDC is displayed. The driving system comprises of two DC motors utilised by the vehicle. These DC motors enable the turning of the sprocket, rotating the chain link, and the idle wheels in the same direction, either clockwise or counterclockwise. Consequently, the robot turns in the corresponding direction while navigating towards the dredging unit.

Assembled hardware for the EPRSDC

Figure 9 showcases the fully assembled hardware design of the EPRSDC. The robot's drive system comprises of two-way units, each with 110 tank tread chain links measuring 450 mm x 412 mm. The tank tread idle wheels were positioned at an angle of 45° to enable the crawler to drive on inclined surfaces. The tank tread sprockets were designed with a like-type chain to enable drive rotation for the crawler with a shaft still torque of 9.88Nm at 100% power.

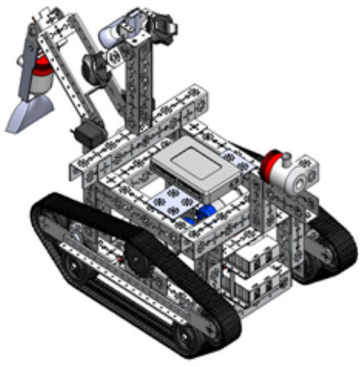

Figure 7—3D design of the electric-powered robotic subsea crawler

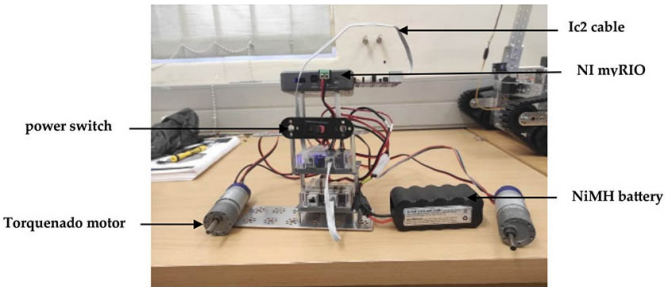

Figure 8—Test benching drive unit and communication system of the crawler

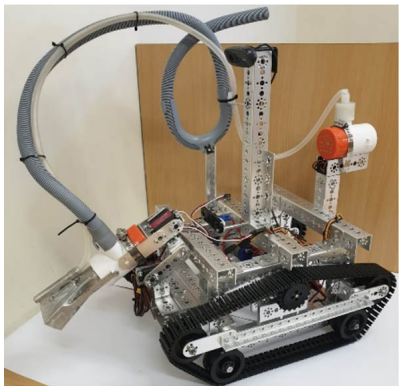

Figure 9—Assembled hardware of the EPRSDC

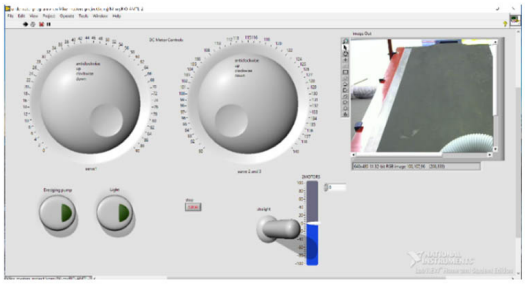

Figure 10—User interface control system platform

To control the robot, NI-myRIO 1900 was used as a controller, and a Logitech c110 webcam was connected to the NI-myRIO for environment visual signal. A laptop was used to communicate with the NI-myRIO via an IP address. The LabVIEW algorithms software was used to operate and control the crawler. The dredging and seabed jetting system pumps were mounted on the crawler arm and back pump base, respectively, using two 12-volt SAIFLO pumps. A two-way relay module, 30A 5–12-volt high low-level trigger relay system was used to control these units. The relay system was connected to a DIP from the NI-myRIO, and a block software was used to connect to the user interface for operation.

Control platform using user interface

Figure 10 displays the controller unit (CU), also known as the user interface, which serves as the software platform for transmitting instructions from the computer to the NI myRIO, enabling the crawler to execute various functions. The knob servo controllers (1, 2, and 3) were utilised to regulate the first and second joints of the two-degree-of-freedom (2-DOF) boom arm. The servo motor was duplicated at the second joint (2 x 25 kgcm) due to the weight of the boom arm (0.548 kg), which gave sufficient torque to lift its weight. The moment of the force acting on the arm was determined by multiplying the total arm length by the weight (0.54 x 15.5 kg), which equalled 8.494kg/cm for the arm with a uniformly distributed load of (0.548 kg). The two-motor control knobs were calibrated from 0% to 100% to lift the arm on the first or second joint, and from -0% to 100% to return the boom arm to its initial position. The slider was used to move the EPRSDC forward from +0% to 100%, and backward from -0% to -100%. The motor controller switch button (straight) enabled the change of the drive system direction (clockwise and counterclockwise). The emergency button was designed to halt the entire control system during operation in the event of software malfunction. The camera system was utilised to send real-time videos and images to the control room, enabling the crawler operator to view the operational environment. The pump and light switches were used to turn the dredging pump on or off.

Figure 11—Final design for the ramp describing the function

Experimental test ramp

As depicted in Figure 11, the experimental setup involved adjusting the ramp to five distinct angles using the two arms, which had holes designed to act as stoppers for the various degrees of inclination (0°, 15°, 20°, 25°, and 30°). After the height adjustment, the crawler was operated to climb the ramp and drive a distance of 1.8 metres. The ramp was fabricated using 25 mm x 25 mm steel tube pipes with a 3 mm thick surface drive sheet. The experimental procedure was conducted three times for each inclination category, and the results were recorded.

Experiment

The obtained outcome presents an experimental evaluation of the EPRSDC's drive performance across a range of ramp inclinations.

Maximum velocity versus different angles of inclination

Recording the maximum velocity at various angles of inclination for the EPRSDC is crucial for optimising its performance and ensuring drive safety, as shown in Table 1. Different angles of inclination simulate diverse terrains and challenges the EPRSDC might encounter. By systematically measuring the maximum velocity at each angle, engineers can determine the crawler's capability to navigate slopes and uneven surfaces.

This data is essential for designing efficient control algorithms, as the crawler's performance can vary significantly based on the incline. Understanding the limitations and capabilities at different angles helps fine-tune the crawler's control systems, allowing for better responsiveness and stability during real-world operations.

Moreover, recording maximum velocities provides insights into the crawler's overall efficiency and power distribution across varying terrains. It aids in the development of predictive models to anticipate performance under different conditions, contributing to the crawler's reliability and adaptability in practical applications in subsea mining activities.

Figure 12 provides a visual representation of the evaluation of the EPRSDC performance. The evaluation specifically focuses on measuring the time it takes for the crawler to cover a ramp distance of 1.8 metres at a 0° angle of inclination. The experiment was carried out under the condition that the crawler was operating at its maximum capacity, which is specified as 100%.

The experiment was conducted three times, for the purpose of ensuring consistency and reliability of the results. After each trial, the time taken for the crawler to cover the specified ramp distance was recorded. The average time taken from these three trials was calculated to be 5.9 seconds.

This information suggests that under the described conditions, the EPRSDC is capable of covering a ramp distance of 1.8 metres

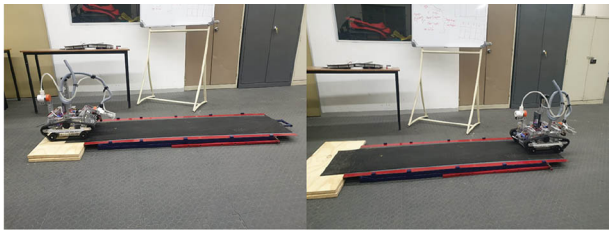

Figure 12—Drive test experiment for EPRSDC at an angle of 0°

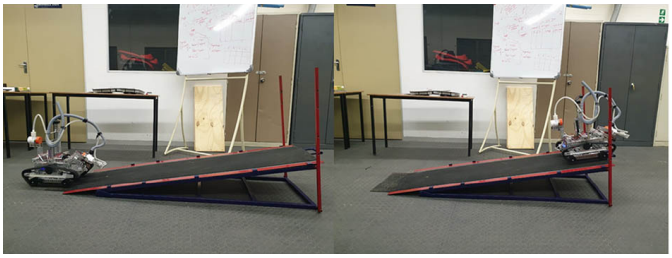

Figure 13—Drive test experiment for EPRSDC at an angle of 15°

Figure 14—Drive test experiment for EPRSDC at an angle of 20°

at a 0° angle of inclination, in an average time of 5.9 seconds when operating at its maximum capacity. This data provide insights into the speed and efficiency of the crawler under these specific conditions, offering valuable information for assessing its performance in real-world applications. Table 1 shows all the drive test result at 0° angle of inclination.

Figure 13 depicts the outcome of a drive test experiment conducted on the EPRSDC with a ramp angle of 150. During this experiment, the crawler was operated at its maximum power output, set at 100%, while covering a distance of 1.8 metres.

The primary parameter measured in this experiment was the time taken to complete the specified task. To ensure reliability, the experiment was conducted three times, and the obtained results were averaged. The average time recorded for the crawler to cover the 1.8-metre distance under the specified conditions was 9.0 seconds.

This information provides insights into the performance of the crawler under specific conditions, particularly at a ramp angle of 15° and operating at maximum power output. The recorded average time can be considered as an indicator of the efficiency and speed of the crawler in completing the assigned task within the given parameters. Table 1 shows the result for the data collected for the test at 15° inclinations.

As seen in Figure 14, the results of a drive test experiment conducted on the EPRSDC over a ramp inclination of 20°. In this experiment, the crawler was operated at its maximum power level, set at 100%. The primary metric measured was the time taken by the crawler to cover a distance of 1.8 metres on the inclined ramp, and three consecutive trials were performed to evaluate the average time taken, as seen in Table 1.

After conducting these trials, the average time taken by the crawler to cover the 1.8-metre distance was calculated. The average time, as stated, was recorded to be 7.2 seconds.

The results suggest that, on average, it took the EPRSDC 7.2 seconds to traverse the specified distance over the 20° inclined ramp when operating at maximum power (100%). This average provides a summary measure of the crawler's performance under these specific conditions.

The results obtained from the drive test experiment on the crawler provide valuable insights into its performance under maximum power conditions and at a specific inclination angle of 25° degrees. The distance covered by the crawler, which was 1.8 metres on the ramp, serves as a critical metric for evaluating its mobility and efficiency in traversing inclined surfaces. By conducting the experiment three times and calculating the average time taken (8.5 seconds), a robust methodology was employed to mitigate potential variability and enhance the reliability of the findings. This repetition not only ensures consistency but also contributes to the overall accuracy of the observed performance metrics, as seen in Table 1.

The scientific significance of these results lies in their applicability to real-world scenarios where crawlers may need to navigate challenging terrains with varying degrees of inclination. The combination of distance covered, and time taken to complete the task provides a comprehensive understanding of the crawler's capabilities, aiding in the optimisation of its design and functionality for specific applications. The experiment's controlled conditions and systematic approach enhance the validity of the outcomes, making them a valuable reference for further research and development in the field of crawler technology and robotics.

The experimental setup depicted in Figure 16 aimed to assess the performance of the crawler under specific conditions, namely at an inclined angle of 30°. This angle was chosen to simulate a scenario where the crawler encounters an inclined surface, requiring it to traverse the incline. The crawler was operated at its maximum power level of 100%, providing a standardised condition for the assessment. The primary metric for performance evaluation was the time taken by the crawler to traverse a predefined distance of 1.8 metres on the inclined ramp. To ensure reliability and minimise variability, the experiment was replicated three times, and the average time taken over these repetitions was determined to be 9.9

Figure 15—Drive test experiment for EPRSDC at an angle of 25°

Figure 16—Drive test experiment for EPRSDC at an angle of 30°

seconds. This averaging approach helps mitigate potential outliers or random fluctuations, providing a more representative measure of the crawler's performance under the specified inclined conditions.

The utilisation of an inclined angle in the experiment is crucial as it introduces an additional challenge to the crawler's locomotion system, simulating real-world scenarios where environmental conditions may not be entirely flat. The choice of maximum power level ensures that the crawler is operating at its peak capacity, allowing for a comprehensive assessment of its capabilities. The repetition of the experiment and subsequent calculation of the average time taken enhance the robustness of the results, contributing to a more reliable evaluation of the crawler's performance under the specified conditions. These methodological considerations contribute to the scientific rigor of the experiment as seen in Table 1, enabling meaningful insights into the crawler's behaviour on inclined surfaces.

Torque versus velocity at a 0° angle of inclination

The relationship between torque and velocity at a 0° angle of inclination is crucial for the study of EPRSDC due to its impacts on their ability to move effectively on the seabed as recorded in Table 2. At this angle, which represents a flat surface, torque becomes more critical for overcoming resistance and obstacles, allowing the robot to generate sufficient force to traverse uneven terrains. In contrast, velocity (speed) may be less important in such scenarios, as the emphasis lies on the robot's ability to exert the necessary torque for efficient movement in a challenging subsea environment.

Figure 17 depicts the relationship between the torque and velocity of the crawler at an angle of inclination of 0°. The experiment involved recording the time taken to cover a distance of 1.8 metres at different torque values. The motor power was varied at five levels using the user interface as follows:

- At 20% maximum power, the crawler did not exhibit any forward movement. This indicates that within the power range of 1% to 19%, the crawler weighing 8.173 kg failed to initiate motion.
- At 40% maximum power, the crawler took 25.7 seconds to complete the 1.8 m drive task.
- At 60% maximum power, the crawler took 12 seconds to complete the 1.8 m drive task.
- At 80% maximum power, the crawler took 7 seconds to complete the 1.8 m drive task.
- At 100% maximum power, the crawler took 6 seconds to complete the 1.8 m drive task.

Torque versus velocity at 20° angles of inclination

Figure 18 displays the correlation between torque and velocity at an inclination angle of 20°. The experiment involved recording the time taken for the crawler to cover a distance of 1.8 metres at various torque values, as presented in Table 3. Motor power was increased to five different levels as follows:

- At 20% of maximum power, the crawler did not exhibit any forward motion. This indicates that within the power range of 1% to 19%, the 8.173 kg crawler was unable to move.
- At 40% of maximum power, the crawler completed the 1.8 m drive task in 41 seconds.
- At 60% of maximum power, the crawler completed the 1.8 m drive task in 15 seconds.
- At 80% of maximum power, the crawler completed the 1.8 m drive task in 9.9 seconds.
- At 100% of maximum power, the crawler completed the 1.8 m drive task in 7 seconds.

Minimum torque versus different angles inclination

Figure 19 and Table 4 collectively demonstrate the minimum torque values corresponding to different inclination angles, as detailed below:

- EPRSDC at 0° inclination with a minimum torque of 30% of the maximum torque.
- EPRSDC at 15° inclination with a minimum torque of 32.6% of the maximum torque.
- EPRSDC at 20° inclination with a minimum torque of 34.3% of the maximum torque.
- EPRSDC at 25° inclination with a minimum torque of 35.6% of the maximum torque.
- EPRSDC at 30° inclination with a minimum torque of 37.3% of the maximum torque.

Result discussion

Ocean driving technology is a complex field that requires a thorough understanding of the relationship between driving efficiency and torque at various angles of inclination. To evaluate the effectiveness of the EPRSDC in driving under different ocean terrains, a series of tests were conducted and the data were recorded in a table. By plotting the data into graphs, it was possible to analyse the results and determine if the EPRSDC is capable of efficiently driving at certain angles of inclinations in different ocean environments.

The following conditions were assumed for EPRSDC:

- There is no slippage between the tank tread chain link and the rubber surface of the ramp.
- The system is considered ideal, meaning that there are no losses and all energy generated by the motor is converted entirely into the translational motion of the driving base.

The rotational torque of the 12-V DC torquenado motor, denoted as N, is calculated based on a rotational speed of 100 RPM, resulting in an angular speed (ω) of 10.47 rad/s. The maximum torque produced by a single motor is 4.94 N/m (700 ozin). Two motors were used for propelling the crawler with a total torque of 9.88 Nm. The power input is determined by multiplying the torque (9.88 Nm) by the angular speed (10.47 rad/s), resulting in a

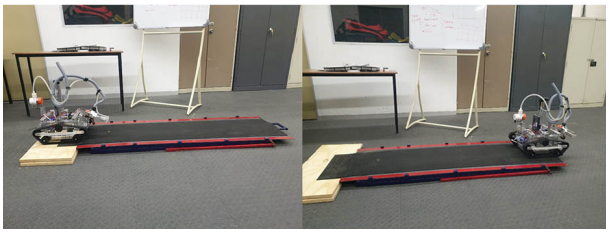

Figure 17—Drive test of EPRSDC at an angle of 0°

Figure 18—Drive test experiment for EPRSDC at an angle of 20°

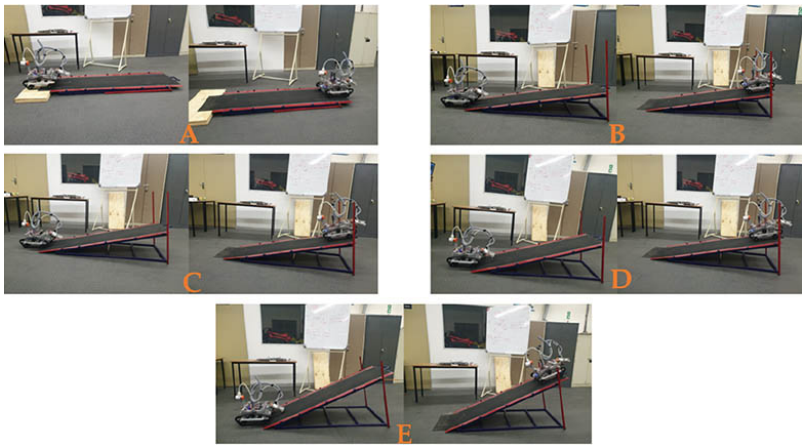

Figure 19—Crawler on different angle of inclination from 0° to 30°

Table 1

Maximum velocity versus different angles of inclination

Distance covered in metres	Time taken (in seconds)	Average time (second)	Maximum velocity (m/s)	Angle of inclination (in degrees)
1.8	6.05 6.17 5.6	5.9	0.305	0°
1.8	7.09 6.96 6.98	7.01	0.256	15°
1.8	7.1 7.3 7.3	7.2	0.250	20°
1.8	7.93 7.71 9.91	8.5	0.211	25°
1.8	9.29 10.2 10.3	9.93	0.181	30°

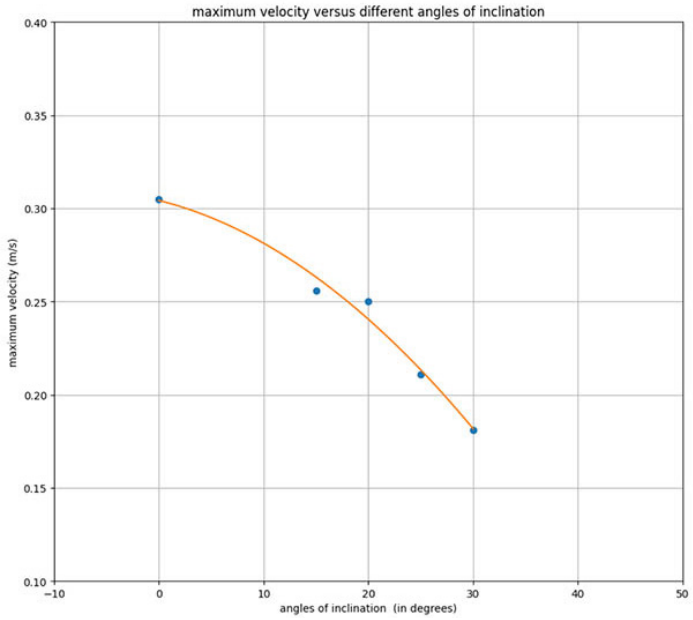

Figure 20—Graph of maximum velocity versus different angles of inclination

Table 2

Torque versus velocity at 0° angles of inclination

Distance covered in metres	Time in seconds	Average time seconds	Torque	Maximum velocity (m/s)	Angle of inclination in degrees
1.8	0, 0, 0	0	20%	0	0°
1.8	25.95 25.33 26.08	25.7	40%	0.07	0°
1.8	12.19 12.03 11.97	12	60%	0.15	0°
1.8	8.00 8.02 7.92	7.9	80%	0.227	0°
1.8	6.05 6.02 6.07	6	100%	0.300	0°

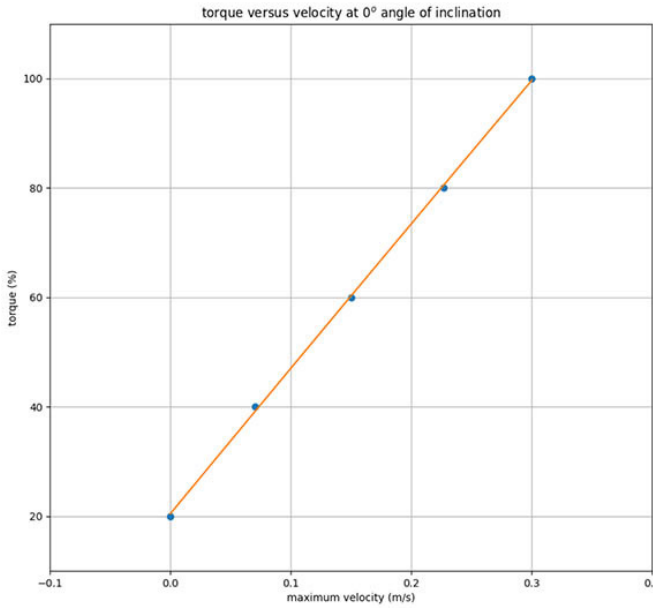

Figure 21—Torque versus velocity at 0º angle of inclination

maximum power of 103.44 watts for the two motors. The efficiency of the system is then calculated as the ratio of power output to power input, where the power output is determined by multiplying the weight (81.73 N) by the velocity.

As shown in Figure 20, the experiment aimed at determining the maximum velocity of the EPRSDC at different angles of inclination. The resulting graph shows a quadratic relationship between the maximum velocity and angle of inclination, with Equation 1:

$$-8.94714809e\text{-}05x^2\text{-}1.39638932e\text{-}03x+ 3.04207745e\text{-}01=0 \quad [1]$$

The data presented in Table 1 shows that the maximum velocity of the crawler decreases as the angle of inclination increases, following a roughly quadratic pattern. For instance, at an inclination angle of 0°, the maximum velocity was 0.305 (high), while at an angle of 30°, it was 0.181 (low). Python was employed to generate a model graph representing the experimental formulas used to solve the quadratic equation.

Figure 21 shows the torque-velocity relationship at a 0° angle of inclination. At maximum power (100%), the crawler achieves its highest torque and velocity of 0.300 m/s. The minimum power required for the crawler, weighing 8.73N, to move forward is 20%. Thus, the crawler's speed can range from 0 to 0.300 m/s, depending on the motor power applied. The torque-velocity graph can be mathematically expressed as a quadratic equation, i.e., Equation 2:

$$-8.93975716\ x^2+266.77666129x+ 20.44560365=0 \quad [2]$$

Figure 22 depicts the correlation between torque and maximum velocity for the subsea crawler at 20° angles of inclination. The graph indicates that the crawler's highest velocity is achieved at 100% full power (torque), with a value of 0.257 m/s. At 20% torque, the minimum velocity is 0 m/s. To overcome the weight of the crawler, which is 8.73N, more than 20% of the maximum motor capacity is required to initiate movement.

The quadratic equation that represents the relationship between torque and maximum velocity at an inclination angle of 200 is shown in Equation 3:

$$-299.07208471x^2+380.67631735x+ 21.49772579=0 \quad [3]$$

The graph depicted in Figure 23 displays the minimum percentage torque required to move the crawler from its stationary

Table 3

Torque versus velocity at 20° angles of inclination

Distance covered in metres	Time taken in (seconds)	Average time (second)	Torque	Maximum velocity (m/s)	Angle of inclination in degrees
1.8	0, 0, 0	0	20%	0	20°
1.8	40.36 41.86 42.39	41.5	40%	0.043	20°
1.8	15.76 15.54 15.65	15.7	60%	0.114	20°
1.8	10.06 9.86 10.02	9.9	80%	0.181	20°
1.8	7.35 7.29 7.46	7	100%	0.257	20°

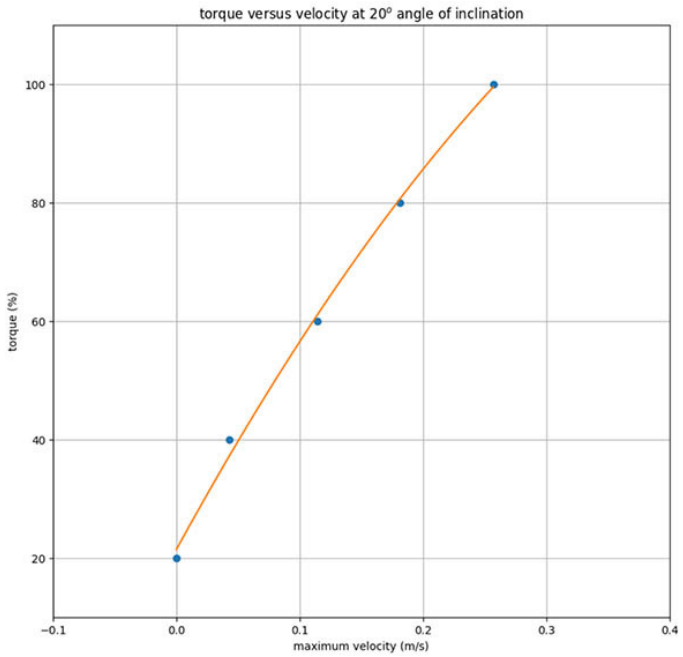

Figure 22—Torque versus velocity at 20° angles of inclination

position under various angles of inclination. The experiment indicates that a minimum of 30% torque is required to set the crawler in motion at 0° angle of inclination. At 30° inclinations, the minimum torque required is 37.3%. The results demonstrate that the minimum torque required to move the crawler varies from 30% to 37.3% of its total torque at different angles of inclination. Thus, a minimum of 30% torque is necessary to overcome the weight of the crawler at different angles of inclination.

The quadratic equation that establishes the relationship between the angle of inclination in degrees and the minimum torque required can be expressed as:

$$3.93720565e\text{-}03\ x^2+1.27095761e\text{-}01x+ 2.99792779e+01=0 \quad [4]$$

The graph depicted in Figure 24 displays the correlation between the efficiency and torque at 0° and 20° angles of inclination. The results indicate that the efficiencies were relatively low at 20% torque and peaked at 100% torque. The crawler had superior efficiency at 0° compared to the efficiency at 20°, indicating that driving the crawler at an angle of inclination of 20° resulted in higher energy losses than at 0°. Moreover, the efficiency curve reached its maximum at 80% torque at 0°, beyond which it began to decline. This implies that increasing the power input (torque) from 80% to 100% does not lead to a further increase in efficiency. The efficiency can only increase from 20% to 80% power on different angles of inclination before it starts to decline.

The quadratic equations for the relationship between efficiency and torque at 0° and 20° angles of inclination are represented by the following formulas:

$$5.03571429e\text{-}05\ x^2 - 8.84285714e\text{-}03\ x - 1.49800000e\text{-}01 = 0 \text{ (for 0° inclination)} \quad [5]$$

$$2.82142857e\text{-}05\ x^2 + 5.88571429e\text{-}03\ x - 1.05600000e\text{-}01 = 0 \text{ (for 20°inclination)} \quad [6]$$

Conclusion

This research involves the development and assembly of a scaled-

down electric-powered subsea robotic crawler using Tetrix Max robotics kits, with the aim of assessing its potential for underwater mining/dredging applications. The performance of the crawler was evaluated using a test ramp that allowed for adjustment of inclination angles ranging from 0° to 30°. Three consecutive tests were carried out for each angle, with the crawler covering a distance of 1.8 metres. The tests were conducted to investigate the crawling characteristics of the system under uneven and sloppy environments. The results of the experiments were recorded, tabulated, and graphically illustrated. The experiments conducted included determining the maximum velocity versus different angles of inclination, the torque versus velocity at 0° and 20°

Table 4

Minimum torque versus different angle of inclination

Distance covered in metres	Minimum torque at full power	Average minimum torque	Angle of inclination (in degrees)
1.8	29% 31% 30%	30.0%	0°
1.8	32% 33% 33%	32.6%	15°
1.8	34% 34% 35%	34.3%	20°
1.8	35% 36% 36%	35.6%	25°
1.8	37% 38% 37%	37.3%	30°

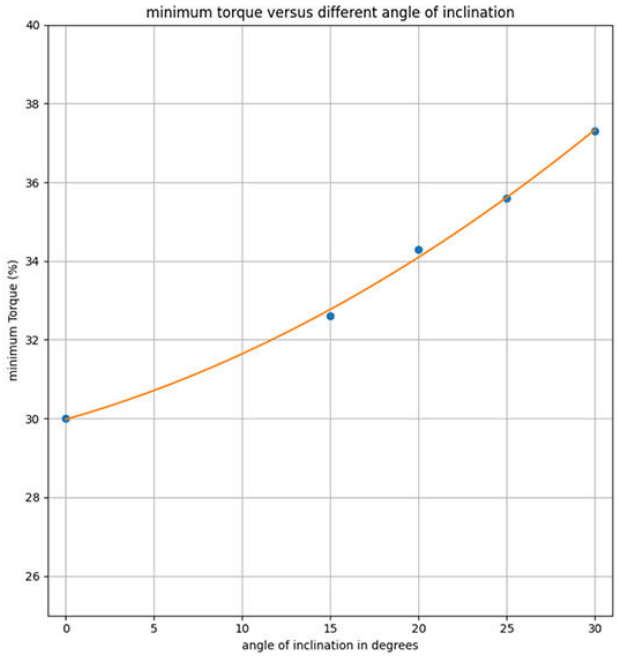

Figure 23—Minimum torque in percentage versus different angle of inclination

Table 5

Graph of efficiency versus torque at 0° angle of inclination

Torque (%)	Average velocity	Useful power output (watts)	Power input	Efficiency (%)
20%	0	0	20.688	0
40%	0.07	5.721	41.376	0.138
60%	0.15	12.255	62.064	0.197
80%	0.227	18.54	82.752	0.224
100%	0.300	24.51	103.44	0.237

Table 6

Graph of efficiency versus torque at 20° angle of inclination

Torque (%)	Average velocity	Useful power output (watts)	Power input	Efficiency (%)
20%	0	0	20.688	0
40%	0.043	3.514	41.376	0.085
60%	0.114	9.317	62.064	0.150
80%	0.181	14.793	82.752	0.179
100%	0.257	21.00	103.44	0.203

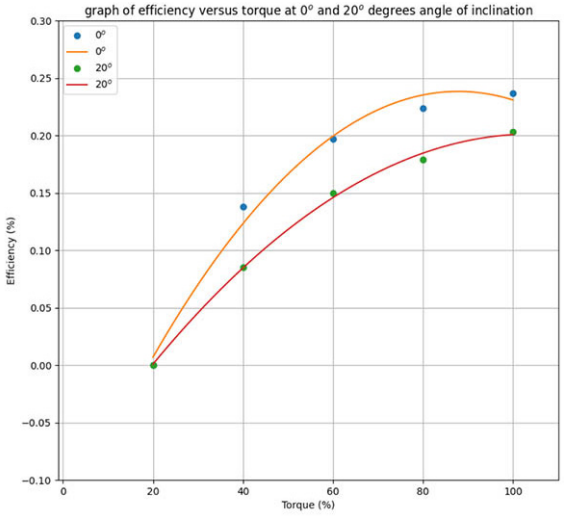

Figure 24—Graph of efficiency versus torque at 0° and 20° angles of inclination

angle of inclination, drive minimum torque versus different angles of inclination, and efficiency versus torque at 00 and 200 angle of inclination. The results show that increasing the angle of inclination decreases the maximum velocity of the crawler, and that more powerful motors are required to overcome steeper angles. The minimum power required to move the crawler was 20% of maximum power at 0° inclination, while at 20° inclinations, at least 34.3% of maximum power was required to overcome the weight of the crawler. The minimum torque required to move the crawler at a 30° inclination was 37.3%. The efficiency of the drive system was higher at a 0° inclination compared to 20° inclinations. These findings provide valuable information for the future development of the electric-powered subsea robotic crawler for underwater mining/dredging applications.

Acknowledgements

We would like to express our sincere gratitude to Cape Peninsula University of Technology for their valuable support and contribution, which played a crucial role in the successful completion of this research. Additionally, we would like to extend our special thanks to Prof. Atanda K. Raji, Dr Efe Orumwense, and other individuals who have provided their valuable guidance and support towards this paper.

Author contributions

Mike Oluwaseun Ojumu: Formulated the design concept, integrated hardware, developed architectural software for the driving system, and wrote the original draft.

Atanda Kamoru Raji: Conducted final data validation, managed project administration, contributed to project conceptualisation, provided supervision, and performed writing review and editing.

Efe Orumwense: Verified the methodology, validated data, visualised the research concept, and conducted writing review and editing.

References

Daanen, H. 2017. Mobility of Subsea Tracked Equipment. delf. Available at: http://repository.tudelft.nl/

Haga, M., Hiroshi, W.,Fujishima, K. 2001. "Digging control system for hydraulic excavator". *Mechatronics*, vol. 11, no. 6, pp. 665–676, 2001, doi: 10.1016/S0957-4158(00)00043-X

Mooney, J.G., Johnson, E.N. 2014. "A Comparison of Automatic Nap-of-the-earth Guidance Strategies for Helicopters," *J.F. Robot.*, vol. 33, no. 1, pp. 1–17, 2014, doi: 10.1002/rob

Naidoo, R.N. 2013. "Global Health Action Mining: South Africa's legacy and burden in the context of occupational respiratory diseases". *Glob. Health Action*, pp. 1–4, Feb. 2013, doi: 10.3402/gha.v6i0.20512

Nazaruddin, Gunawan, 2015. "(PDF) Undercarriage Design of Excavator Model in Application of Various Track Drive," Researchgate, pp. 1–7, Dec. 2015, Accessed: Jul. 30, 2021. [Online]. Available: https://www.researchgate.net/publication/320557845_Undercarriage_Design_of_Excavator_Model_in_Application_of_Various_Track_Drive

Tondolo, N.L. 2012. "Quantitative investigation of hydraulic equipment failures within the original equipment manufacturer standard," *Creat. common*, pp. 1–75.

Van Bloois, J. Willem, J. Frumau, S.S. 2009. Ocean Mining: Deep Sea Mining: A New Horizon for Dredging Technology," *OTC Offshore Technol. Conf.*, pp. 1–1, May 2009, doi: 10.4043/20047-MS ◆